VII International Conference on Particle-Based Methods
PARTICLES 2021
P. Wriggers, M. Bischoff, E. Oñate, A. Düster & T. Zohdi (Eds)

DEVELOPMENT OF MPS METHOD FOR ANALYSING CONVECTION AND SOLIDIFICATION OF MULTI-COMPONENT CORIUM IN SEVERE ACCIDENT OF A LIGHT WATER REACTOR

TAKANARI FUKUDA[1*], AKIFUMI YAMAJI[1], XIN LI[1], JEAN-FRANÇOIS HAQUET[2] AND ANNE BOULIN[2]

[1] Waseda University, Shinjuku 3-4-1, Tokyo, Japan
E-mail: sun-village@akane.waseda.jp

[2] CEA, DES, IRESNE, DTN, SMTA, Severe Accident Modeling Laboratory,
Cadarache F-13108 Saint-Paul-Lez-Durance, France

Key words: MPS, Severe Accident of a Nuclear Reactor, Molten Core-Concrete Interaction (MCCI), Multi-Phase Convective Flow, Solidification

Abstract. In this study, a numerical approach for analyzing the internal status of Molten Core-Concrete Interaction (MCCI) has been developed based on Moving Particle Semi-implicit (MPS) method. Among the key required models, such as accurate viscosity interaction model for solidifying particles and interface tension models of different liquid phases, preliminary attempts have been made with new models. Namely, a simple mixing model and gas hosting particle model has been implemented to simulate the experiment with affordable calculation cost. The analysis results for VULCANO VF-U1 experiment have shown the possible mechanisms responsible for the characteristic distribution of the solidified metallic corium, which seemed to be highly dependent on the density of surrounding oxidic corium

1 BACKGROUND AND OBJECTIVE

In a severe accident of a nuclear reactor, the molten core, or "corium" (lava-like mixture of molten core materials composed by oxidic (UO_2, ZrO_2, etc.) and metallic (Fe, Zr, Ni, etc.)) phases, might breach the Reactor Pressure Vessel and relocate on the concrete substrate of a containment vessel. Subsequently, the so-called Molten Core-Concrete Interaction (MCCI) might take place, which involves heat generation by the oxidic corium due to decay reactions (e.g., Beta decay) of unstable isotopes, thermal decomposition of the concrete with the gas release, concrete melting (ablation), mixing of molten concrete with the oxidic corium, and oxidation of the metallic corium. The multi-phase melt convection may last for several days until the melt cools down and solidifies [1]. From the viewpoints to mitigate, manage and evaluate severe accidents, there have been extensive MCCI experiments and numerical analyses of MCCI, which mainly focused on the concrete ablation behavior and the concrete decomposition gas release [2].

Meanwhile, following the accident at Fukushima Daiichi Nuclear Power Plant (from hereinafter "1F"), evaluation of the post-MCCI debris distribution has become important for evaluating the current status of the damaged reactors and planning debris retrieval from 1F.

Thus, the necessity to deepen our understanding of the post-MCCI corium internal status has become evident. However, few studies have been carried out with such a standpoint.

More recently, French Alternative Energies and Atomic Energy Commission (CEA) performed an MCCI experiment called "VULCANO VF-U1" using 1F prototypic corium. According to the post-MCCI investigation of internal distribution, (1) most metallic debris were distributed from the bottom concrete (basemat) interface to the lower parts of the sidewall interfaces; (2) some metallic fragments were found in the middle of the oxidic phase; (3) a part of the metallic corium protrudes into the oxidic corium as depicted in Figure 1 [3].

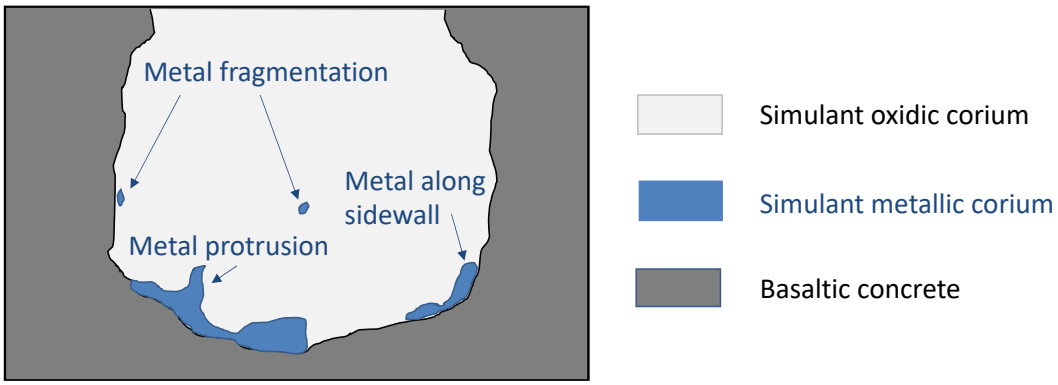

Figure 1 The schematic view of the post-MCCI investigation of VULCANO VF-U1 [3] [4]

To investigate possible reasons for such characteristic debris distribution, CEA used Volume Of Fluid (VOF) method to perform isothermal analysis of corium flow for the first 10 seconds and succeeded to show the generation of metallic droplets scattered by concrete decomposition gas and localization of continuous metallic due to interface tensions [4]. However, this analysis did not consider the heat transfer or phase changes (melting and solidification) among the oxides, metals and concrete. To reveal the mechanism responsible for the characteristic post-test distribution of VULCANO VF-U1, the following phenomena should be considered during the evaluation of the multi-component melt interfaces. Namely, (1) gradual solidification of corium over the mushy zone (between the liquidus and solidus temperatures); (2) influences of the concrete decomposition gas bubbles on the oxidic and metallic corium convection; (3) the ablation of the concrete and the mixing of molten concrete with the oxidic corium phase.

Moving Particle Semi-implicit (MPS) method is a Lagrangian-based particle method, which is suitable to track the complex interface dynamics with heat transfer involving solid-liquid phase changes. However, the past MCCI analyses with MPS method focused on the concrete ablation with limited analyses of the multi-component convective flow involved during MCCI [5, 6, 7, 8]. Neither influence of the interface tension, nor that of the above given three important phenomena on the multi-component distributions of the melt has been investigated, partly because of lack of numerical accuracy and models, which were needed to address such issues. Hence, in this study, we aim to develop an MCCI analysis method based on MPS method which incorporates physical models for above-described key phenomena. Moreover, through analyses of the developed MPS method, we aim to show the mechanism responsible for the characteristic distribution of the solidified metallic phase observed in VULCANO VF-U1.

2 NUMERICAL METHODS

2.1 Governing Equations, Algorithm and Discretization Methods

The governing equations required for MCCI simulations are the mass, momentum and energy conservation lows for incompressible fluid, described as:

$$\nabla \cdot \boldsymbol{u} = 0 \tag{1}$$

$$\rho \frac{D\boldsymbol{u}}{Dt} = -\nabla P + \mu \nabla^2 \boldsymbol{u} + \rho g + \boldsymbol{F}_{IT} \tag{2}$$

$$\frac{DH}{Dt} = k\nabla^2 T + Q \tag{3}$$

where $\boldsymbol{u}$ is the velocity vector field, ρ is the density of the fluid, t is time, μ is viscosity, g is gravity acceleration, $\boldsymbol{F}_{IT}$ is interface tension, H is specific enthalpy, k is thermal conductivity, T is temperature and Q is a volumetric heat source. The viscosity and thermal conductivity between two particles are calculated by the harmonic mean, as commonly approximated [9].

When computing Eq. (2) , viscosity is implicitly calculated at the end of every time step to prevent "numerical creep". Otherwise, raising viscosity never terminates the flow (the melt never fully solidifies), because velocity is given without influence of viscosity after the pressure term calculation in the ordinary MPS algorithm [10]. Some of the drawbacks of this algorithm are the enlarged discretization error and numerical instability caused by the distorted particle distribution due to the unguaranteed incompressibility. Hence, adoption of techniques to reduce discretization error becomes important, such as the Second-order Corrective Matrices (SCM) developed by Duan et, al., [11], as follows:

$$\langle \nabla \phi \rangle_i = \frac{1}{n_0} \sum_{j \neq i} \left[w_{ij} \frac{\phi_j - \phi_i}{r_{ij}} \left(\begin{pmatrix} \boldsymbol{C_1} \\ \boldsymbol{C_2} \end{pmatrix} \boldsymbol{P} \right) \right] \tag{4}$$

$$\langle \nabla \cdot \boldsymbol{A} \rangle_i = \frac{1}{n_0} \sum_{j \neq i} \left[w_{ij} \frac{\boldsymbol{A}_j - \boldsymbol{A}_i}{r_{ij}} \cdot \left(\begin{pmatrix} \boldsymbol{C_1} \\ \boldsymbol{C_2} \end{pmatrix} \boldsymbol{P} \right) \right] \tag{5}$$

$$\langle \nabla^2 \phi \rangle_i = \frac{2}{n_0} \sum_{j \neq i} \left[w_{ij} (\phi_j - \phi_i) \frac{(\boldsymbol{C}_3 + \boldsymbol{C}_4)\boldsymbol{P}}{l_0 r_{ij}} \right] \tag{6}$$

where the triangular brackets "< >" imply that the derivative term inside is approximated by the revised particle interaction model. The subscripts i and j are particle indexes, ϕ_i and $\boldsymbol{A_i}$ are arbitrary scalar and vector variables, respectively, r_{ij} and w_{ij} are the distance and weight function value between particle i and j, n_0 is the initial particle density and $\boldsymbol{C}_k$ $(k = 1,2,3,4)$ is SCM (The details should be found in [11]). Furthermore, the Particle Shifting (PS) technique [12] was applied to improve the numerical stability by recovering regular particle alignment from distorted distribution.

2.2 Physical Models for MCCI simulation

2.2.1 Solidification and Melting Model

Viscosity change and immobilization of the fluid during solidification or melting is modeled with the value solid fraction γ, which is defined as:

$$\gamma = \begin{cases} 1 & (H < H_s) \\ \dfrac{H_l - H}{H_l - H_s} & (H_s \leq H \leq H_l) \\ 0 & (H_l < H) \end{cases}$$

where H_s and H_l are the enthalpy corresponding to the solidus and liquid temperature, respectively. The melting of concrete is modeled as follows. A concrete particle is treated as a liquid particle when its solid fraction is below the threshold γ_T. Then, the liquid viscosity is assumed to change exponentially with solid fraction, represented by the blue line in Figure 2. On the other hand, the solidification process of corium is modeled in three steps as represented by the red lines in Figure 2. For a corium particle, when $\gamma < \gamma_T$, the viscosity changes as a function of solid fraction in the same manner as that of concrete. When the solid fraction reaches the predetermined threshold γ_T, the viscosity is increased to a predetermined large value. The velocity of the corium particle should be largely diffused by the large viscosity and eventually decrease to 0. In order to save calculation cost for solving such highly viscous flow, the coordinate of the corium particle is fixed when its velocity is below a sufficiently small threshold value (2×10^{-3} m/s assumed in the current study).

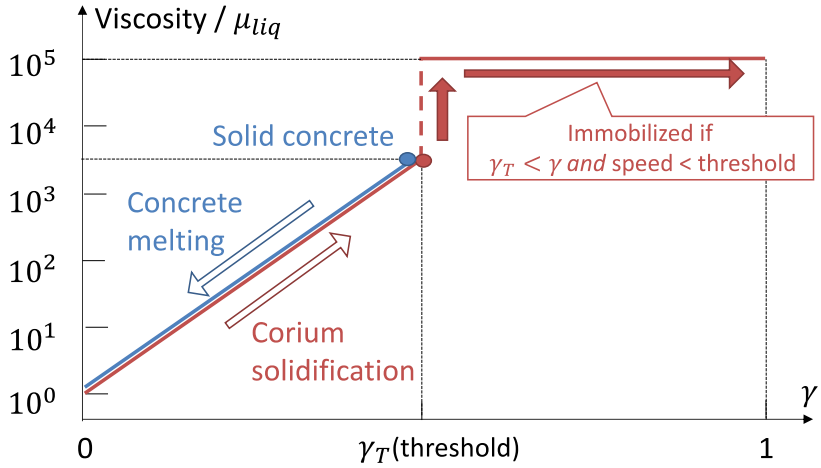

Figure 2 Viscosity change through the processes of melting and solidification

2.2.2 Interface Tension Model

For modeling the interface tension between two different liquid phases (e.g., metallic and oxidic corium), this study employs the inter-particle potential interface tension model developed by Zhu et, al., [13]. With this model, interface tension $\boldsymbol{F}_{IT}$ in Eq. (2) is expressed as the gradient of the potential energy among particles as:

$$\boldsymbol{F}_{IT}(\boldsymbol{r}) = -\nabla \mathrm{P(r)} \tag{7}$$

where P(r) is:

$$P(r) = \begin{cases} \frac{C}{3}\left(r - \frac{3}{2}r_{min} + \frac{1}{2}r_e\right)(r - r_e)^2 & (0 \le r < r_e) \\ 0 & (r_e \le r) \end{cases} \quad (8)$$

Here, r_{min} is tentatively set as $1.5l_0$. For the methodology to determine the fitting parameter C between two different particles, readers may refer to [13].

2.2.3 Gas Release Model

Direct simulations of bubble dynamics have been extensively studied with MPS method successfully [14]. However, due to the requirement of very small time-step to stably calculate liquid-gas interface, which typically involves about 1000 times-different density jump, the required calculation cost is large. Hence, it is still difficult to explicitly model gas bubbles for the simulation of large MCCI experiment, which lasts for a long time (in the order of hours). Hence, in this study, a new "gas host particle" model has been developed to consider the expected influence of concrete decomposition gas on the flow and distribution of the metallic phase.

Firstly, as shown in Figure 3, if a solid concrete particle reaches the H_2O vaporization temperature of 373K, one of the "molten" corium particles (namely, $\gamma < \gamma_T$) is randomly chosen from the effective interaction range to be a "gas host particle", which is regarded as partly gas and partly corium (The idea of gas particle host is partly from [8]). With this treatment, gas host particles can have a density with the same order of magnitude as that of the corium. Thus, it enables stable calculation with affordable time-step interval.

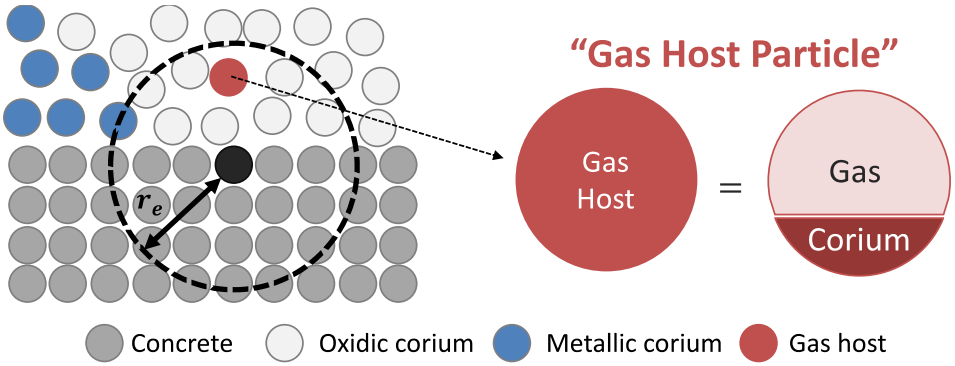

Figure 3 Image of gas host particle model

Then, the generated gas host particles would rise due to the buoyancy force. When the gas host particles rise beyond a predetermined height in the corium pool (tentatively set as 1cm below the top surface of the corium pool), they will be regarded as having released gas to the atmosphere and be reverted to the original corium type.

2.2.4 Molten Concrete-Oxidic Corium Mixing Model

As molten concrete, mainly composed of SiO_2, Al_2O_3 and CaO, is miscible with oxidic corium, a new model to consider their mixing has been developed, based on the concept proposed by Chai et, al., [7]. In this model, a molten concrete particle becomes an oxidic corium

particle if the number of neighboring molten oxidic corium is more than half of the total number of neighboring particles, as shown in Figure 4.

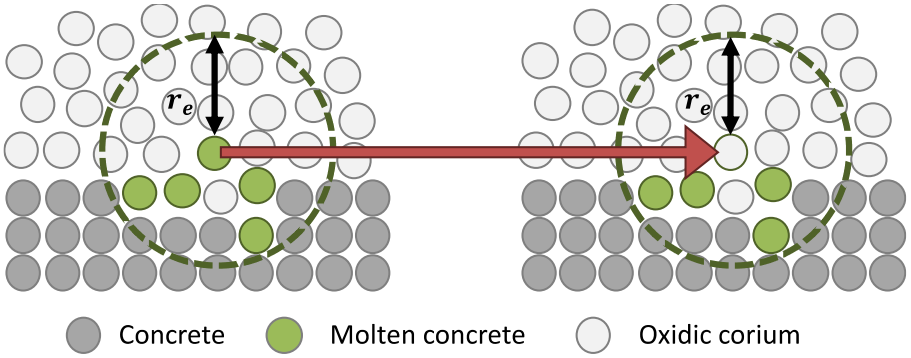

Figure 4 Image of molten concrete-oxidic corium mixing model

To ensure the mass and energy conservation during the mixing, the physical properties of oxidic corium, such as density and specific heat, are averaged as follows:

$$\phi_{MixedOxide} = \frac{\phi_{InitialOxide} N_{InitialOxide} + \phi_{InitialConcrete} N_{InitialConcrete}}{N_{InitialOxide} + N_{InitialConcrete}} \quad (9)$$

where ϕ represents density or specific heat, N is the number of particles. Subscript "MixedOxide" means the updated properties of oxidic corium, which has mixed with molten concrete. The subscript "InitialOxide" means the initial oxidic corium before mixing with the molten concrete. The subscript "InitialConcrete" means the properties of molten concrete which has not mixed into oxidic corium yet.

As explained above, this study assumes that the oxidic corium particles mix with the neighboring molten concrete particles instantaneously and the resulting distributions of the properties are assumed to be uniform. In reality, mixing happens with some finite diffusion process. Consideration of the finite diffusion process during the mixing should be addressed in the future.

3 ANALYSIS CONDITION

3.1 Configuration and Material properties

VULCANO VF-U1 was one of the MCCI experiments carried out in VULCANO facility of CEA, France. The experiment was designed to investigate the concrete ablation behavior in the 1F accident [3]. The test section was a full cylindrical crucible with an inner diameter of 250 mm and a height of 200 mm as depicted in Figure 5 (a). The concrete type was basaltic, which was the same as that of the 1F primary containment vessel floor. Before the start of the induction heating, the simulant corium powder composed of UO_2, CaO stabilized ZrO_2 and Zr were filled in the cavity. The 304L stainless-steel spheres modeling metallic corium were initially located in the simulant corium powder at 70 mm above the basemat of the cavity.

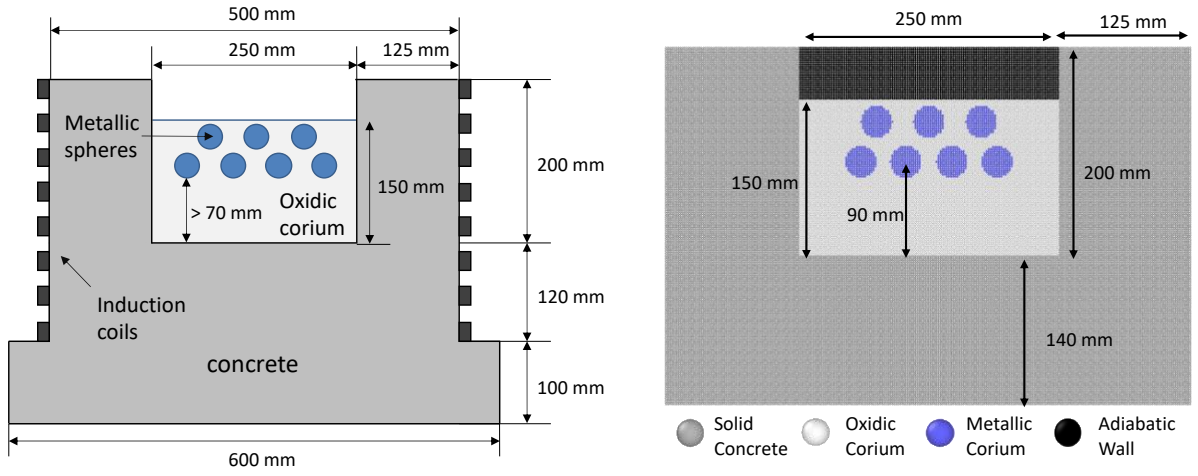

Figure 5 (a) Cross-section view of the test section and (b) particle configuration for MPS simulation

Two-dimensional MPS analyses have been conducted by configuring the experimental test section by particles with a diameter of 2.0 mm, as shown in Figure 5 (b). The particle size was determined to capture the local convections and the metallic droplets scattering by the gas bubbling with affordable calculation cost. The full cylindrical crucible of the experiment represented by the two-dimensional (2-D) geometry. As shown in Figure 5, the 2-D geometry corresponds to the cross section of the cylindrical crucible through the center. Thus, there are some differences between the two geometries, such as the surface area to volume ratio. In this study, the upper surface of the corium pool is covered by an adiabatic virtual wall, to suppress the numerical instability due to pressure calculation of the free surface. Air cooling and radiation from the free surface of the corium pool are neglected, which should be addressed in future study. Moreover, the consideration of oxidation of the metallic corium is also one of the remaining targets.

The material properties used in this simulation are summarized in Table 1 and the tentatively assumed interface tension coefficients are summarized in Table 2. Since the solidus/liquidus temperature of corium depends on mixed concrete content, the solidus/liquidus temperature of oxidic corium is assumed to depend on the volumetric fraction of concrete, x, as follows:

$$T_{solidus} = \begin{cases} 2790 - \dfrac{2790 - 1350}{0.15} x \ (0 < x < 0.15) \\ 1350 \ (0.15 < x < 1) \end{cases} \tag{10}$$

$$T_{liquidus} = \begin{cases} 2790 - \dfrac{2790 - 2500}{0.3} x \ (0 < x < 0.3) \\ 2500 \ (0.3 < x < 0.8) \\ 1650 + \dfrac{2500 - 1650}{0.2} (1 - x) \ (0.8 < x < 1) \end{cases} \tag{11}$$

where, 2790 is the liquidus temperature of oxidic corium [3], 1350 and 1650 are the solidus/liquidus temperature of pure basaltic concrete [15]. The value of 2500 and the form of Eq.(10) and Eq.(11) are approximately determined from the empirical correlation in [16].

Table 1 Summary of material properties [4] [15] [3] [17] [18]

Material	Oxidic Corium	Metallic Corium	Concrete	Molten Concrete	Gas Host
Density [kg/m^3]	6312 *1	6461	2400	2400	1000*3
Dynamic Viscosity [Pa·s] *2	0.0194	0.00475	-	0.0194*4	0.0194 *4
Thermal conductivity [W/mK]	1.5	25	1.5 *4	1.5 *4	1.5 *4
Specific heat capacity [J/kgK]	498	600	950	950	498 *4
Solidus/Liquidus Temp.[K]	2790/2790	1673/1723	1350/1650	1350/1650	N/A
Latent Heat [J/kg]	3.67×10^5	2.80×10^5	5.18×10^5	N/A	3.67×10^5 *4
γ_T	0.55	0.55	0.33	0.33	N/A
Contact angle [°]	90*3	←	-	90*3	←

*1 Change depending on the concrete content. *2 The value for complete liquid ($\gamma = 0$) particles. For the particle with $0 < \gamma < \gamma_T$, the dynamic viscosity is determined as $\mu = \mu_{liq}\exp(2.5C_r\gamma)$ [19]
*3 Tentatively assumed value. *4 Tentatively same as that of oxidic corium.

Table 2 Tentatively assumed interface tension coefficient between every pair of materials

	M-A	**O-A**	**C-A**	**G-A**	**M-O**	**O-G**	**H-M**	**M-C**	**O-C**	**C-H**
$\boldsymbol{\sigma}$ [N/m]	0.75	0.05	0.25	0.25	0.25	0.25	0.5	0.5	0.25	0.25

(M, O, C and G stand for metallic corium, oxidic corium, molten concrete and gas host particle, respectively)

3.2 History and Treatment of Injection Heating

Figure 6 shows the history of the net injected power (i.e., after the power conversion efficiency has been considered) in the test section of the experiment [3]. Based on the temperature data obtained in the experiment, the MPS simulation has been performed from the time of 3840 seconds after the start of the experiment. However, until the time of 4422 seconds, the simulant corium powder was mostly solid. Hence, from the time of 3840 to 4422 seconds, only the heat calculation of Eq. (3) has been performed, without solving the fluid flow. From hereinafter, the time of 4422 seconds in the experiment is regarded as 0 second (initial condition) in the current MPS analysis.

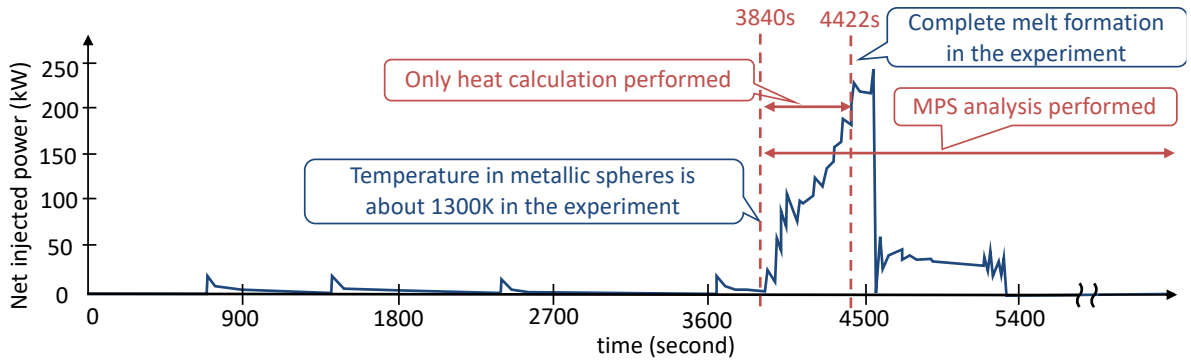

Figure 6 History of the heat injection to the test section of VULCANO VF-U1

In the current MPS simulations, the net injected power is assumed to be uniformly dissipated to all the liquid particles without any losses by heat loss to the environment. Moreover, as explained in Section 3.1, the 2-D calculation geometry underestimates the surface area to volume ratio of the real geometry. Thus, the net injected power in the simulation was reduced by a factor of 0.64 to account for the differences.

4 RESULTS AND DISCUSSIONS

4.1 When the Melt Density is Updated with the Mixing Model

The results described in this section is obtained from analyses, which assumed that the density is updated when the oxidic melt is mixed with the molten concrete as modeled by Eq. (9) described in Section 2.2.4. Figure 7 shows the snapshots of the MPS simulation results. Soon after the beginning of the simulation, the metallic corium relocated to the bottom of the cavity, because its density was higher than that of the oxidic melt. As shown for t = 130 seconds, the metallic – oxidic interface was disturbed by rising of the gas host particles from the concrete. Then, as concrete ablation proceeded (300 s - 800 s), the density stratification interface became clear, because of significant density reduction of the oxidic corium due to mixing with the molten concrete. By 2000 s, both the concrete ablation and the overall corium flow almost terminated, giving the final distribution as shown in Figure 7.

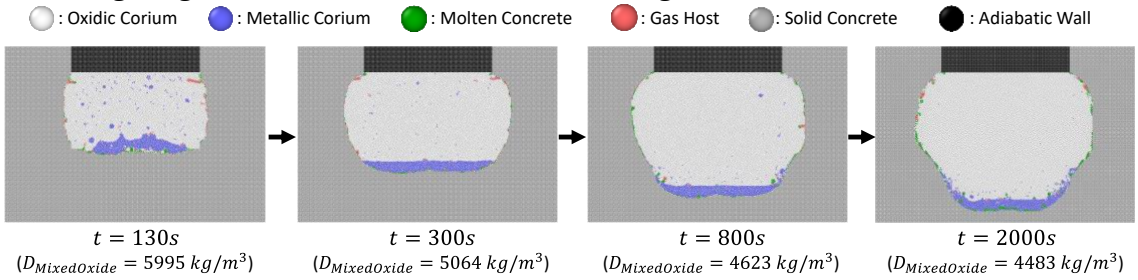

Figure 7 Snapshots of the result with complete mixing of molten concrete and oxidic corium

A noticeable characteristic of the mixed corium pool distribution is that the peripheral part of the metallic corium was distributed along the concrete sidewall after about 600 seconds. Figure 8 shows the profiles of compositions and solid fraction around the peripheral metallic corium part at 662 seconds. As can be seen from Figure 8, the peripheral part of the metallic corium layer (marked by the dotted line circle) is precedingly cooled and solidified since the oxidic corium part above the peripheral part of it is significantly cold due to the large heat flux to the concrete sidewall. Hence, the solidified peripheral metallic part is “left behind” on the

concrete sidewall from the subsidence of the main body of the metallic layer due to the efficient heat transfer from the highly conductive metallic corium layer.

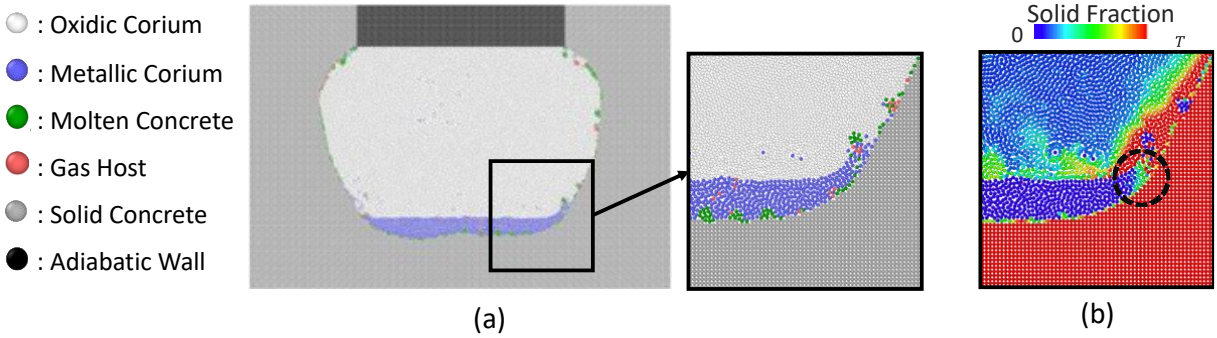

Figure 8 (a) Composition distributions and (b) solid fraction distribution around the peripheral metallic corium part at t = 662 s

4.2 When the Melt Density Does Not Change by Mixing

The metallic corium distribution along the concrete sidewall shown in Section 4.1 somewhat agrees with that of the experiment depicted in Figure 1. However, the analysis results do not reproduce the metal fragments or protrusion observed in the experiment. Moreover, the ablation profile of the concrete crucible in the experiment is rounder than that was obtained by the MPS simulation. These differences seem to indicate that convection of the metallic phase was more pronounced and the heat flux to the concrete was more uniformly distributed in the experiment than those simulated by the MPS method.

Such difference might be attributed to overestimation of the density difference between the oxidic and metallic corium, especially around the metallic corium. This is because, as described in Section 2.2.4, the mixing between the oxidic corium and molten concrete is modeled to occur instantaneously and uniformly in this study. Thus, a comparison case in which the density of the oxidic corium does not decrease during the mixing has been analyzed, aiming to check the influence of the density of oxidic corium on the metallic corium distribution. Figure 9 shows the snapshots of the result without reduction of the oxidic corium density during mixing. The fragmentation of metallic corium is more pronounced compared to the results in Figure 8, because of the smaller density difference between the oxidic and metallic phases.

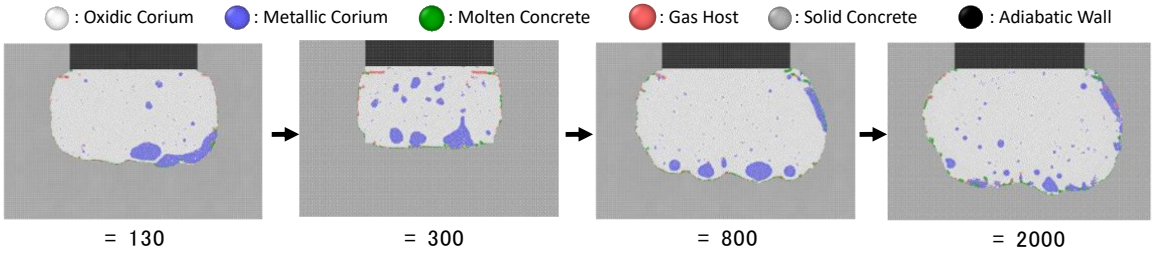

Figure 9 Snapshots of the result WITHOUT density reduction of oxidic corium through Mixing

Moreover, the metal distribution on the concrete sidewall and the protrusion of the metallic corium into the oxidic corium is also reproduced. Figure 10 shows the solid fraction profile around the metallic corium part at 590 s. In Figure 10, part of the metallic corium “crawls up” vertically (marked by the square in Figure 10), which can be explained as follows. The concrete surface in touch with the metallic corium receives intense heat flux from metallic phase, due to

the high thermal conductivity of the metallic corium. Consequently, concrete ablation in such areas is enhanced, leading to generation of more gas bubbles and molten concrete, which "drag" the metallic corium upward along the sidewall. Then, the metallic corium is kept in the gap between concrete sidewall and solidified oxidic corium due to the capillary effect. Finally, the metallic corium is trapped in very viscous (or solidified) oxidic corium layer.

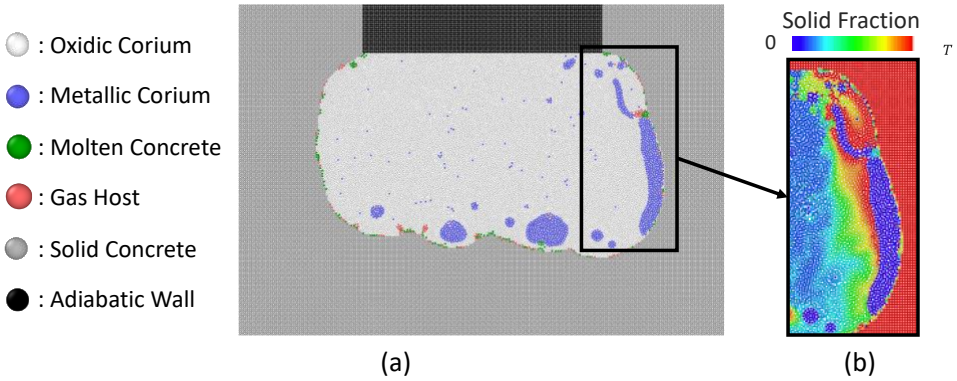

Figure 10 (a) Composition distributions and (b) solid fraction distribution around metallic corium at t = 590 s

Thus, comparisons of the results obtained in Section 4.1 and 4.2 may also highlight discussions regarding density difference of the oxidic and the metallic layers. That is, if density difference between the oxidic and metallic corium is not significant, the distribution of the metallic phase can be dominated by the local upward convection and the interface tension (capillary force).

5 CONCLUSION

In this study, we have developed the integrated full-timescale MPS-MCCI analysis and showed the mechanisms which might be responsible for the characteristic distribution of the solidified metallic phase found in post-test investigation of VULCANO VF-U1 experiment. Namely, convective flow induced by molten concrete and gas bubbles, and interface tension (capillary force) between the oxidic and the metallic corium. However, as the results were found to be highly dependent on the density of the oxidic corium, improvement of the mixing model is one important remaining issue.

ACKNOWLEDGEMENT

This work was supported by JSPS KAKENHI Grant Number JP21J12226. The MPS code of the present study was developed based on MMPS-HDDM code that was kindly provided by G. Duan and A. Yamaji.

REFERENCES

[1] J. Rohde and G. Cenerino, "Ex-vessel melt behavior and its role in safety assessment of LWR," in Second OECD (NEA) CSNI Specialist Meeting on Molten Core Debris-Concrete Interactions, 1992.

[2] OECD/NEA, "State-of-the-Art Report on Molten Corium Concrete Interaction and Ex-Vessel Molten Core Coolability," 2017.

[3] V. Bouyer, et, al., “LARGE SCALE VULCANO MOLTEN CORE CONCRETE INTERACTION TEST CONSIDERING FUKUSHIMA DAIICHI CONDITION,” in The 9TH European Review Meeting on Severe Accident Research (ERMSAR2019), Prague, 2019.
[4] J. F. Haquet, et, al., “A local multiphase approach for the modelling of nuclear severe accident using CFD methods,” in 10th International Conference on Multiphase Flow, Rio de Janeiro, 2019.
[5] X. Li and A. Yamaji, “A Numerical Study of Isotropic and Anisotropic Ablation in MCCI by MPS Method,” Progress of Nuclear Energy, vol. 90, pp. 46-57, 2016.
[6] X. Li and A. Yamaji, “Three-dimensional numerical study on the mechanism of anisotropic MCCI by improved MPS method,” Nuclear Engineering and Design, vol. 314, pp. 207-216, 2017.
[7] P. Chai, et, al., “Numerical simulation of 2D ablation profile in CCI-2 experiment by moving particle semi-implicit method,” Nuclear Engineering and Design, vol. 301, p. 15–23, 2016.
[8] P. Chai, et, al., “Numerical simulation of MCCI based on MPS method with different types of concrete,” Annals of Nuclear Energy, vol. 103, p. 227–237, 2017.
[9] T. Kawahara and Y. Oka, “Ex-vessel molten core solidification behavior by moving particle semi-implicit method,” Journal of Nuclear Science and Technology, vol. 49, no. 12, p. 1156–1164, 2012.
[10] G. Duan, et, al., “A novel multiphase MPS algorithm for modeling crust formation by highly T viscous fluid for simulating corium spreading,” Nuclear Engineering and Design, vol. 343, p. 218–231, 2019.
[11] G. Duan, et, al., “The truncation and stabilization error in multiphase moving particle semi-implicit method based on corrective matrix: Which is dominant?” Computers and Fluids, vol. 190, pp. 254-273, 2019.
[12] G. Duan, et, al., “An accurate and stable multiphase moving particle semi-implicit method based on a corrective matrix for all particle interaction models,” International Journal for Numerical Methods Engineering, vol. 1, pp. 1-28, 2018.
[13] Y. Zhu, et, al., “Verification and validation of MPS potential force interface tension model for stratification simulation,” Annals of Nuclear Energy, vol. 148, p. 107753, 2020.
[14] R. Chen, et, al., “Current achievements on bubble dynamics analysis using MPS method,” Progress in Nuclear Energy, vol. 118, 2020.
[15] E. R. Copus and D. A. Powers, “Interaction Between a Superheated Uranium Dioxide Jet and Cold Concrete,” in Second OECD (NEA) CSNI Specialist Meeting on Molten Core Debris-Concrete Interactions, 1992.
[16] C. Spengler, et, al., “Assessment and Development of Molten Corium Concrete Interaction Models for the Integral Code ASTEC,” in EUROSAFE Forum For nuclear safety, Brussels, 2005.
[17] T. Dinh, et, al., “Core Melt Spreading On A Reactor Containment Floor,” Progress in Nuclear Energy, vol. 36, no. 4, pp. 405-468, 2000.
[18] V. Strizhov, et, al., “An Assessment of the CORCON-MOD3 Code,” U.S. Nuclear Regulatory Commission, 1996.
[19] M. Ramacciotti, et, al., “Viscosity models for corium melts,” Nuclear Engineering and Design, vol. 204, p. 377–389, 2001.